RASopathy Network Symposium 2021

Alteration of myocardial structure and function in RAF1-associated Noonan syndrome

Saeideh Nakhaei-Rad[1,2], Farhad Bazgir, Marcel Bucholzer, Fereshteh Haghighi, Julia Dahlmann, Anne Schänzer, Andreas Hahn, Sebastian Kötter, Denny Schanze, Ruchika Anand, Florian Funk, Andrea Borchardt, Annette Vera Kronenbitter, Jürgen Scheller, Roland P. Piekorz, Andreas S. Reichert, Marianne Volleth, Matthew J. Wolf, Lukas Cyganek, Bruce D. Gelb, Marco Tartaglia, Joachim Schmitt, Martina Krüger, Martin Zenker, George Kensah, Mohammad R. Ahmadian

[1]Institute of Biochemistry and Molecular Biology II, Medical Faculty of the Heinrich-Heine University, Düsseldorf, Germany; [2]Stem Cell Biology and Regenerative Medicine Research Group, Institute of Biotechnology, Ferdowsi University of Mashhad, Mashhad, Iran

Abstract

RASopathies, including Noonan syndrome (NS), are caused by germline variants in genes encoding components of the RAS-MAPK pathway. Distinct variants, such as the recurrent Ser257Leu substitution in RAF1, are associated with severe hypertrophic cardiomyopathy (HCM). Here, we explored as part of the NS phenotype the elusive mechanistic link of NS-associated RAF1^{S257L} to HCM using three-dimensional cardiac bodies and bioartificial cardiac tissue, differentiated from -patient-derived (RAF1, Ser257Leu) induced pluripotent stem cells (iPSCs). The results revealed molecular, cellular, structural and functional impacts on the myocardium, and elucidated the link of RAF1^{S257L} hyperactivity to hypertrophic myocardial remodeling. Strikingly, electron micrographs of the Z-line area revealed the shortening of I-bands in both iPSC-derived RAF1^{S257L} cardiomyocytes and a cardiac biopsy of a NS patient, linked to which may be caused by aberrant phosphorylation of the giant intra-sarcomeric protein Titin. Remarkably, this phenotype was reverted by using the MEK inhibitor PD0325901. Collectively, our findings uncovered a direct link between a RASopathy gene variant and abnormal sarcomeric structure and cardiac function forming the basis for future therapeutic approaches.

Characterization of generated induced pluripotent stem cells-RAF1^{S257L}

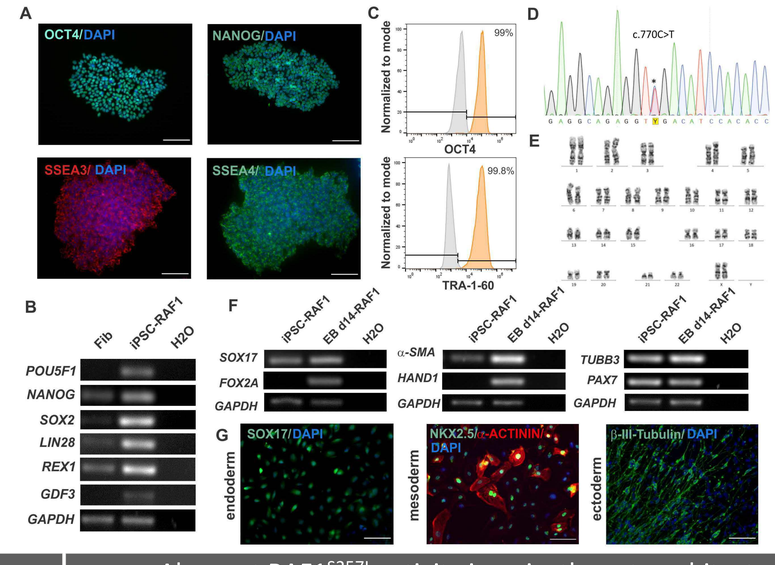

Figure 1. Human iPSC-RAF1^{S257L} reveals expression of pluripotency markers, a normal karyotype, and differentiation potency towards ectodermal, endodermal and mesodermal derivatives in vitro.
A) iPSC-RAF1^{S257L} stain positive for OCT4, NANOG, SSEA3 and SSEA4.
B) RT-PCR analysis of pluripotency markers in iPSCs and control fibroblasts.
C) Flow cytometry analysis confirmed more than 99% of iPSCs stain positive for OCT4 and TRA-1-60.
D) Sanger sequencing confirmed the heterozygous RAF1$^{S257L/+}$ variant in iPSCs (asterisk).
E) iPSCs show a normal diploid karyotype.
F, G) Trilineage differentiation of iPSC-RAF1^{S257L}. Expression of endodermal (SOX17 and FOX2A), mesodermal (α-SMA, HAND1, NKX2.5, and sarcomeric alpha-actinin) and ectodermal (TUBB3 and PAX7); Scale bar, 200 µM.

3D cardiac differentiation of iPSCs with WNT signaling modulation

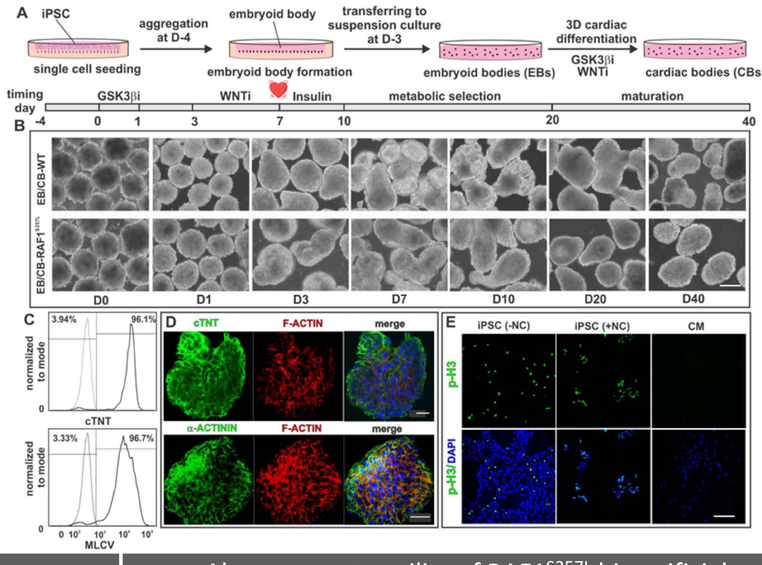

Figure 2. A) Schematic overview of embryoid body (EB) formation using agarose microwells combined with the stages and time lines of EBs differentiation to cardiac bodies (CBs).
B) Light microscopic pictures of EBs/CBs during cardiac differentiation. Scale bar, 200 µM.
C) Flow cytometric analysis of dissociated CBs displayed efficient cardiac differentiation towards ventricular cardiomyocytes by analysis of MLCV2 and cTNT positive cells.
D) Representative immunofluorescence staining of a CB for cTNT and α-actinin expression. Scale bar 20 µM.
E) Illustration of mitotic cells stained with phospho-histone 3 (p-H3) in iPSC cells and CM. Scale bar, 200 µM.

Signaling events in RAF1^{S257L} cardiac bodies

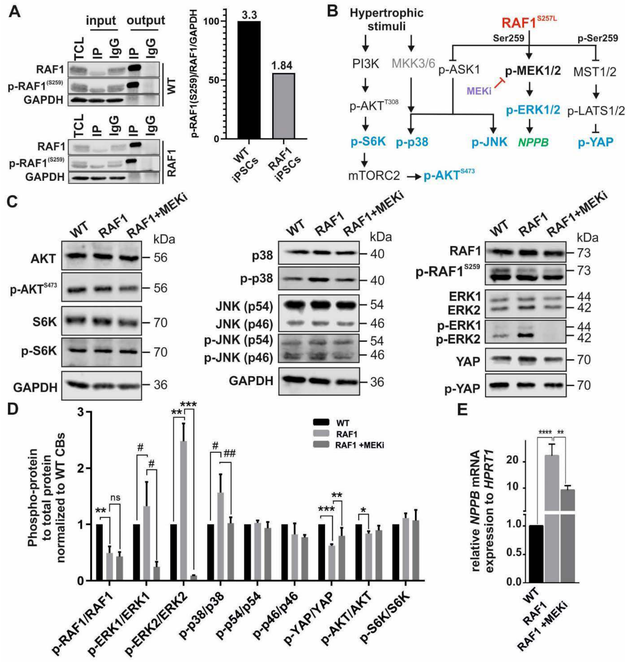

Figure 3. A) Immunoprecipitation and quantification of total and p-RAF1S259 in WT and RAF1^{S257} iPSCs. B) Schematic diagram summarizing the signaling molecules investigated downstream of hypertrophic stimuli and RAF1.
C) Immunoblot analysis of p-AKT vs. AKT, p-S6K vs. S6K, p-RAF1259 vs. RAF1, p-ERK1/2 vs. ERK1/2, p-YAP vs. YAP, p-p38 vs. p38, and p-JNK vs. JNK using cell lysates from WT and RAF1^{S257} CBs (d24).
D) Phospho-protein vs. total protein ratio quantification of three independent experiments as shown in C. *P < 0.05, **P < 0.01, ***P < 0.001, ****P < 0.0001, unpaired 2-tail t-test. # P < 0.05, ## P < 0.01, unpaired 1-tail t-test. n≤2.
E) Quantitative real-time PCR (qPCR) analysis showed significant upregulation of NPPB in RAF1^{S257L} CBs, which was partially reverted in the presence of MEKi, unpaired 2-tail t-test, n=3.

Aberrant RAF1^{S257L} activity impairs the cytoarchitecture of cardiomyocytes

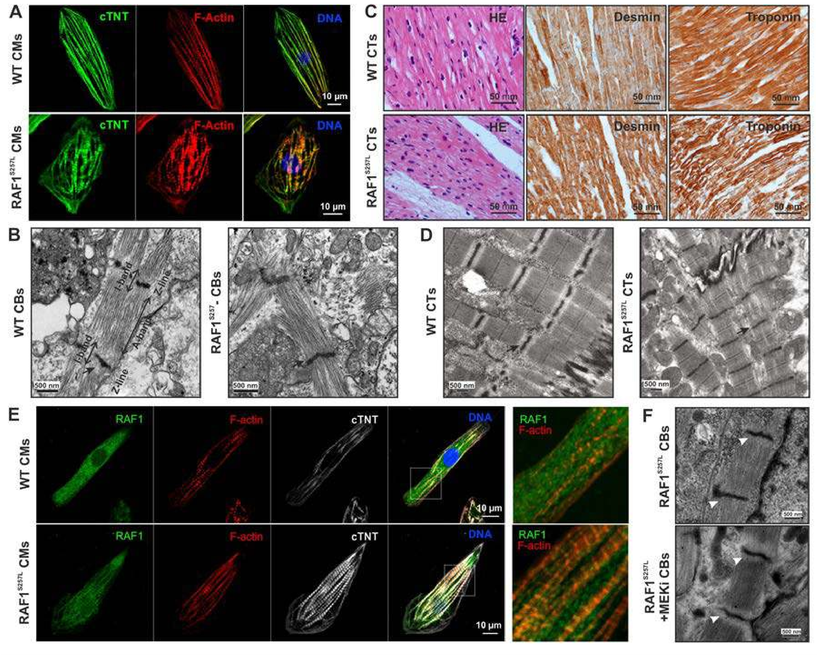

Figure 4. A) Dissociated cardiac bodies were seeded on Geltrex-coated coverslips for seven days and stained for cTNT and F-actin (Scale bar, 10 µm). RAF1^{S257L} CMs exhibited less oriented, more disarrayed, and shorter myofilaments as compared to WT CMs
B) Representative EM images from RAF1^{S257L} cardiac bodies (CBs) revealed a stronger myofibrillar disarray.
C) IHC analysis of RAF1^{S257L} cardiac tissue (CTs) from one of the NS individuals with RAF1 c.770C>T varian for desmin and troponin showed microfilament disarray.
D) Representative EM images of the same RAF1^{S257L} CTs as in C.
E) Representative ICC images of RAF1^{S257L} and WT CMs at d90 post-differentiation showed RAF1 co-localization with cTNT and F-actin at the sarcomere (Scale bar, 10 µm).
F) EM images of RAF1 mutated RAF1^{S257L} CBs (d40) treated with 0.2 µM MEK inhibitor (PD0325901) from d12 of differentiation.

Aberrant contractility of RAF1^{S257L} bioartificial cardiac tissue

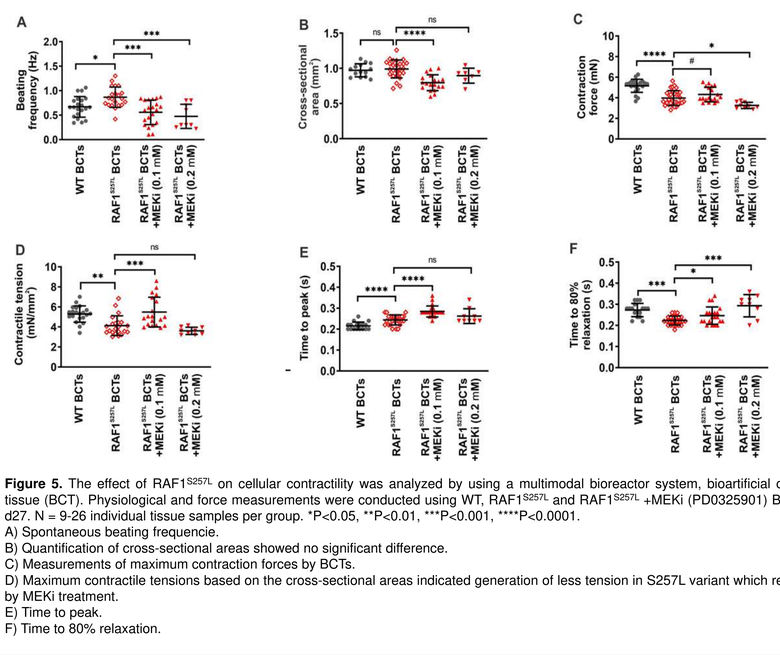

Figure 5. The effect of RAF1^{S257L} on cellular contractility was analyzed by using a multimodal bioreactor system, bioartificial cardiac tissue (BCT). Physiological and force measurements were conducted using WT, RAF1^{S257L} and RAF1^{S257L} +MEKi (PD0325901) BCTs at d27. N = 9-26 individual tissue samples per group. *P<0.05, **P<0.01, ***P<0.001, ****P<0.0001.
A) Spontaneous beating frequencie.
B) Quantification of cross-sectional areas showed no significant difference.
C) Measurements of maximum contraction forces by BCTs.
D) Maximum contractile tensions based on the cross-sectional areas indicated generation of less tension in S257L variant which rescued by MEKi treatment.
E) Time to peak.
F) Time to 80% relaxation.

Conclusions

Collectively, here we demonstrated new aspects of RAF1 function in human iPSC-derived CMs, which resemble the observed *in vivo* phenotype from the corresponding individual, especially changes in the ultra-structure of the sarcomeres. The S257L variant in RAF1 CMs modulate RAF1-dependent signaling network, fetal gene program, contraction abnormality, calcium transients, and the sarcomeric structures.

- RAF1^{S257L} is hyperactivated and promotes MAPK signaling in cardiomyocytes.
- RAF1^{S257L} is linked to the elevated contraction frequency and reduced contractile tensions of 3D cardiac tissues.

Acknowledgements

This study was supported by the German Federal Ministry of Education and Research (BMBF) – German Network of RASopathy Research (GeNeRARe, grant numbers: 01GM1902A, 01GM1902C 01GM1519D,); the European Network on Noonan Syndrome and Related Disorders (NSEuroNet, grant number: 01GM1602A, 01GM1602B); the International Research Training Group 1902 Intra- and Interorgan Communication of the Cardiovascular System (IRTG 1902-P6); and the German Research Foundation (Deutsche Forschungsgemeinschaft or DFG) through the Collaborative Research Center 974 (SFB 974) "Communication and Systems Relevance during Liver Injury and Regeneration ".